

## Modeling steel moment frame and braced frame buildings in three dimensions using FRAME3D

S. Krishnan<sup>1</sup>

<sup>1</sup> *Asst. Professor, Dept. of Civil Engineering, California Institute of Technology, Pasadena, USA*  
Email: [krishnan@caltech.edu](mailto:krishnan@caltech.edu)

### ABSTRACT :

A procedure for the efficient three-dimensional nonlinear time-history analysis of steel framed buildings is derived. It incorporates three types of nonlinear beam elements - the plastic hinge type, the elastofiber type, and the 5-segment modified elastofiber type – and nonlinear panel zone elements to model yielding and strain-hardening in moment frames, and buckling in braced frames. Floors and roofs of buildings are modeled using 4-node elastic diaphragm elements. The procedure utilizes an iteration strategy applied to an implicit time-integration scheme to solve the nonlinear equations of motion at each time-step. Geometric nonlinearity is included. The plastic hinge beam element consists of two nodes at which biaxial flexural yielding is permitted, leading to the formation of plastic hinges. Elastic rotational springs are connected across the plastic hinge locations to model strain-hardening. Axial yielding is also permitted. A normalized PMM interaction surface is calculated for one of the model sections, and used to characterize the axial force-biaxial moment interaction for all model sections. The panel zone element consists of two orthogonal panels forming a cruciform section. Each panel may yield and strain-harden in shear. The elastofiber beam element is divided into three segments - two end nonlinear segments and an interior elastic segment. The cross-sections of the end segments are subdivided into fibers. Associated with each fiber is a nonlinear hysteretic stress-strain law for axial stress and strain. This accounts for coupling of nonlinear material behavior between bending about the major and minor axes of the cross-section and axial deformation. While beams and columns in moment-frames can be modeled using the elastofiber beam element, braces and columns susceptible to buckling may be modeled using a modified elastofiber beam element with the elastic segment in the standard elastofiber beam element subdivided into two elastic segments and a central nonlinear segment. First mode buckling in the element is simulated through yielding of the central nonlinear segment. All these elements are integrated into a building analysis program, FRAME3D. The various elements and the program are validated against analytical solutions of simple problems, as well as scaled and full-scale tests of beam-column assemblies and 4-6 story structures.

### KEYWORDS:

Nonlinear analysis, moment-frames, braced-frames, panel zone, plastic yielding, fracture, buckling, collapse.

### 1. THE ANALYTICAL MODEL

Modeling nonlinear behavior of steel buildings requires nonlinear beam-column elements that can capture plastic yielding and connection fracture, brace elements that can simulate local and global buckling as well as fracture, panel zone elements that can model shear yielding in joints, and geometric updating to capture P- $\Delta$  effects. The three-dimensional nonlinear analysis program FRAME3D, developed for this purpose, has been founded on over two decades of steel research by Prof. John Hall of Caltech and his students (Hall & Challa 1995, Hall 1995 & 1998, Gan & Hall 1998, Carlson 1999, and Krishnan & Hall 2006a, 2006b). The structural model consists of dispersed nodes in 3-D space that map out the skeleton of the structure. Beam, column, and brace elements interconnect the nodes to form the structural skeleton (Figure 1). A 3-D panel zone element, consisting of six attachment points (labeled a – f in figure), is located centered on each node to model the beam-column-brace joints. This element consists of two rectangular panels that are constrained to remain perpendicular to each other and form a cruciform section. Two of the six attachment points and the node points are collinear, and fall on the line of intersection of the two panels. These two attachment points (e and f), located at the top and the bottom of the cruciform joint, serve as connecting points for columns above and below the joint, respectively. The other four attachment points are located at the mid-points of the edges of

the two panels and serve as connecting points for beams. Braces, when present, are attached to a panel corner at either end. The panel corners are chosen so as to minimize the length of the brace. This rule ensures that the braces oriented in either principal direction of the building connect to the panel that is oriented in that direction, and lie in the plane of the corresponding braced frames. Floor slabs are modeled using elastic plane-stress elements that connect directly to the node points. There are eight global degrees of freedom associated with each node, three translations in the global X, Y, and Z directions, and five rotational degrees of freedom, a rigid body twist of the joint, and two rotations in each of the two panels (rotation of chords a-b & e-f in panel (1), and rotation of chords c-d & e-f in panel (2)). The rotations are in the panel zone coordinate system  $XYZ$ . The nonlinear equations of motion associated with the global degrees of freedom are numerically solved using an iteration strategy applied to an implicit time-integration scheme at each time-step. Full geometric updating is included in both static and dynamic analyses. This involves updating the locations of the joint nodes, attachment points, and the local beam nodes, as well as the orientations of the local element coordinate systems and beam elements.

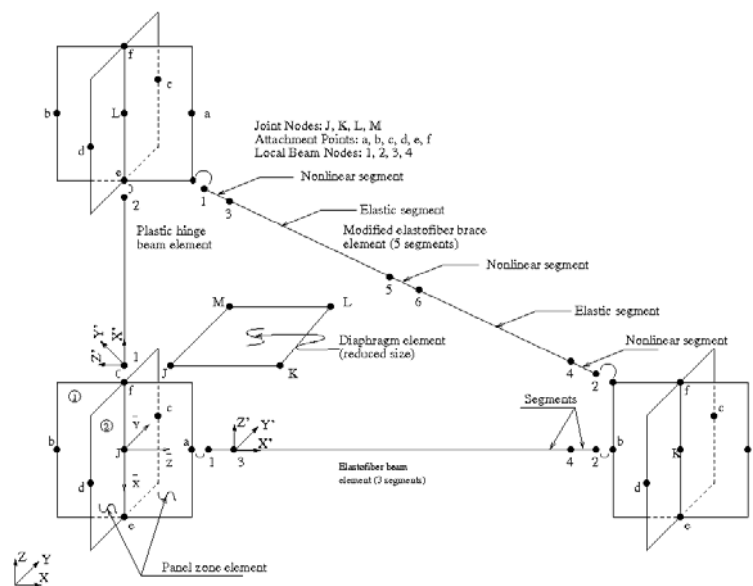


**Figure 1:** Element arrangement in the FRAME3D modeling framework, showing joint nodes, attachment points, beam internal nodes, and the three coordinate systems,  $XYZ$  (global),  $X'Y'Z'$  (element/segment local),  $\bar{X}\bar{Y}\bar{Z}$  (panel zone local). Also shown are the plastic hinge and elastofiber elements for beam/column modeling, the 5-segment modified elastofiber element for brace/slender-column modeling, the panel zone element for joint modeling, and the diaphragm element for floor slab modeling.

### 1.1. Panel Zone Element

Joints, comprising of a length of column within the depth of the connecting beams, are modeled using panel zone elements consisting of two rectangular panels which are perpendicular to each other, panel (1) in the  $\bar{X}-\bar{Z}$  plane and panel (2) in the  $\bar{X}-\bar{Y}$  plane, forming a cruciform section (Figure 2). The thicknesses of all web plates and web doubler plates of the associated column are combined to form the thickness of panel (1), while the thicknesses of all flange plates of the associated column are combined to form the thickness of panel (2). Each panel has two DOF that are also global DOF:  $\theta_Y^B$  &  $\theta_Y^C$  for panel (1), and  $\theta_Z^B$  &  $\theta_Z^C$  for panel (2), where J is the global node at the center of the joint. These rotations deform the two panels into parallelograms, and each pair accommodates a rigid rotation of the corresponding panel about its normal plus its shear deformation. The B and C indicate that the rotating panel edges are connected to columns and beams, respectively. Strain or rotation in one of the panels causes a rigid body rotation but no strain in the orthogonal panel. Material nonlinearity in each panel is included by assuming a linear-quadratic shear stress-strain backbone behavior until ultimate shear stress is reached, and perfectly plastic behavior thereafter, as first proposed by Hall and Challa (1995). Hysteresis

loops, defined by linear segments and cubic ellipses, and hysteresis rules, based on an extended Masing's hypothesis, are used to model the cyclic response of each panel.

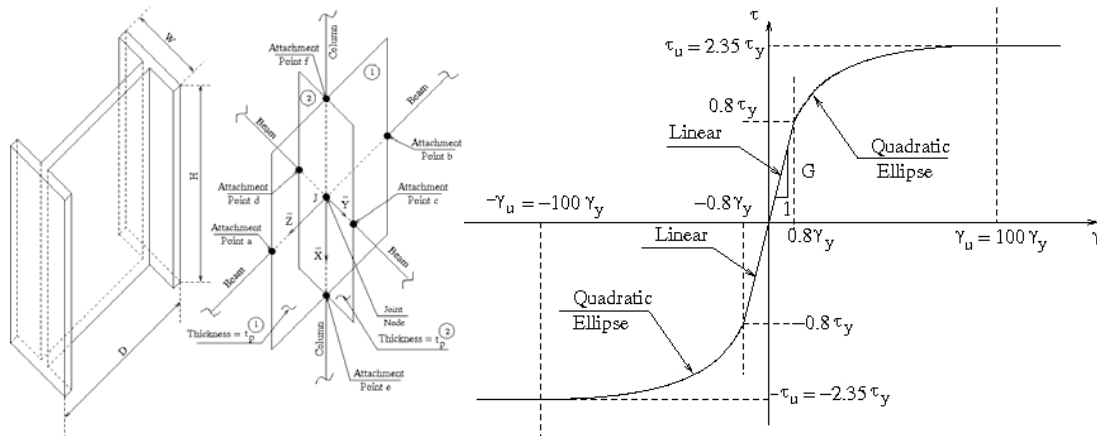


**Figure 2:** Panel zone element located at each joint of the structural model. The element consists of two orthogonal panels that deform in shear. A linear-quadratic backbone curve is used model the shear behavior.

### 1.2. Plastic Hinge Element

The plastic hinge beam element (Figure 3) has two nodes which connect to the attachment points of the panel zone element. Each node has six DOF, three translational and three rotational. Two types of material nonlinearity are considered, axial yielding and major- & minor- axis flexural yielding when the moment reaches the corresponding plastic moment capacity which is a function of the axial force. After flexural yielding, further loading causes a kink, termed a plastic hinge, to form in the beam at that node. Between these plastic hinge locations, the beam behaves elastically. To approximate the effect of strain hardening, elastic rotational springs are mounted across the plastic hinges to exert moments proportional to the kink angles about the Y' and Z' axes.

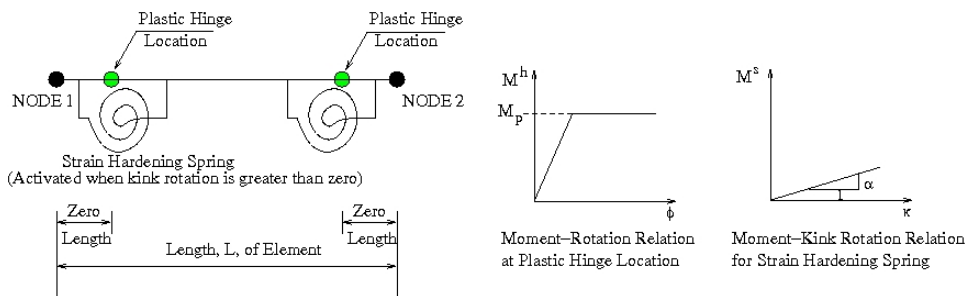


**Figure 3:** Plastic hinge element to model beams and columns.

### 1.3. Elastofiber Element

Fiber elements have been successfully implemented to more accurately account for nonlinear material behavior under combined bending and axial load, including PMM interaction, strain hardening, cracking, and spread of nonlinearity along the member. Fully discretized fiber elements are computationally demanding, especially when implemented in a three-dimensional framework, and a hybrid elastofiber element was recently introduced (Krishnan and Hall 2006b) to alleviate this demand. The elastofiber beam element has three segments and four nodes (Figure 4). The two exterior nodes, 1 and 2, coincide with one of the six attachment points on the adjacent panel zone elements at the left and the right. The two interior nodes, 3 and 4, delineate the two end fiber segments from the elastic middle segment, which is an elastic version of the plastic hinge element, i.e., no axial yielding and no plastic hinging. Each fiber segment is discretized into 20 fibers that run the entire length of the segment. Associated with each fiber is a nonlinear hysteretic stress-strain law, proposed by Hall and Challa (1995), for axial stress,  $\sigma_n$ , and axial strain,  $\epsilon_n$ , where "n" denotes the n<sup>th</sup> fiber. This hysteresis model defines a backbone curve consisting of a

linear portion, a yield plateau, a strain-hardening region which is described by a cubic ellipse, and a strain softening region described by a continuation of the same cubic ellipse. The backbone curve is characterized by seven parameters: yield stress  $\sigma_y$ , ultimate stress  $\sigma_u$ , Young's modulus  $E$ , strain at initiation of strain hardening  $\epsilon_{sh}$ , strain at ultimate stress  $\epsilon_u$ , rupture strain  $\epsilon_r$ , and the tangent modulus at initiation of strain hardening  $E_{sh}$ . Hysteresis loops consist of linear segments and cubic ellipses, and the hysteretic rules to define the cyclic response of each panel are given by Challa (1992). A fiber fracture capability, in the form of a general probabilistic description of the fracture strain, has been added to approximately represent fracture of welded beam-to-column connections Hall (1995, 1998). When the fiber strain reaches the fracture strain, it fractures and can no longer take tension, but upon reversal of loading the fractured and separated parts can come in contact, and the fiber is able to resist compression again. The fiber segment is based on the finite element method, wherein the beam translations and rotations are interpolated linearly and independently from their nodal values, requiring a one-point integration on the shear terms to prevent locking. Each of the four nodes of the elastofiber element have 6 degrees of freedom, three translational and three rotational. The interior nodes are assumed massless, and this allows for static condensation to be performed on the associated DOF, labeled 1-12 in the figure. Within each global iteration, an iterative local member structural analysis is performed to determine the displacements of the interior nodes and the member stresses, strains, and tangent stiffness. The coordinates of the two interior nodes as well as the member orientation are updated after each member iteration.

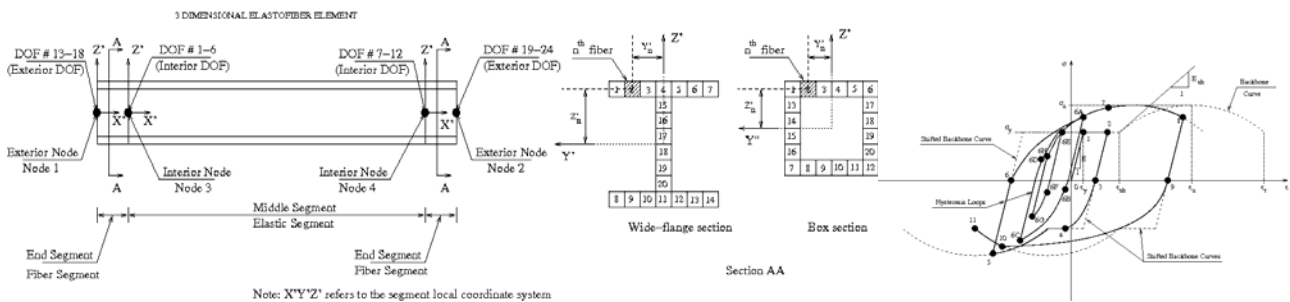


Figure 4: Elastofiber element to model flexure dominated beams and columns.

#### 1.4. Modified Elastofiber (MEF) Element

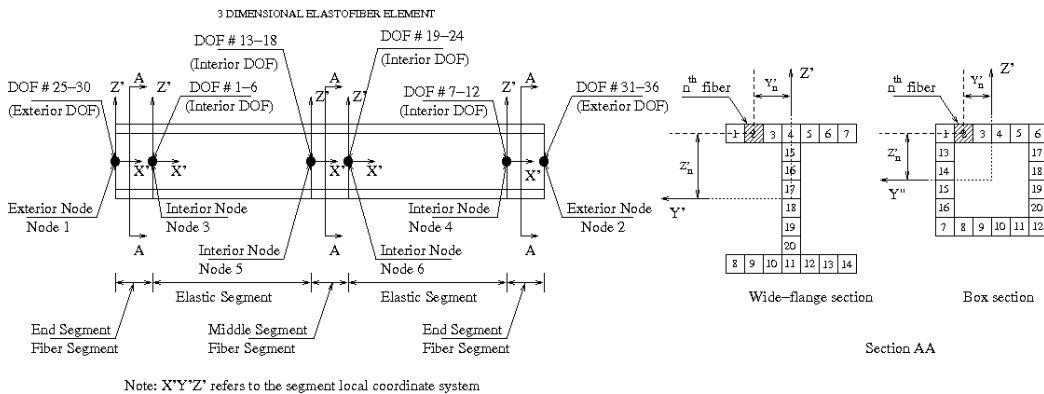


Figure 5: Modified elastofiber element to model buckling-sensitive columns and braces.

While the elastofiber element is able to accurately capture nonlinear behavior at the ends of beams and columns, capturing nonlinear behavior (buckling and cracking) at the middle of braces and slender columns requires the insertion of an additional central fiber segment. This modification to the elastofiber element leads to a 5-segment element with three fiber segments, two at the ends and one in the middle (Figure 5), separated by two interior segments modeled as elastic plastic hinge elements, i.e., with no axial yielding or plastic hinging. Each of the six nodes of the MEF element have 6 degrees of freedom, three translational and three rotational. As for the elastofiber element, the interior nodes are assumed massless, and static

condensation is performed on the associated DOF, labeled 1-24 in the figure. Updating the coordinates of the four interior nodes at the end of each local member iteration allows for the simulation of buckling in the member. As the member deforms, the fibers in the middle segment yield and/or fracture, mimicking local buckling and cracking in the member.

### 1.5. Diaphragm Element

This element is used to model the in-plane stiffness of floor slabs. It is essentially a 4-node plane-stress element connecting to joint nodes J, K, L, and M (Figure 1). Details of the diaphragm element are given by Krishnan (2003). Its behavior is linearly elastic.

## 2. COMPONENT VALIDATION

### 2.1. Large Deflection of an Elastic Cantilever Beam (Krishnan and Hall, 2006b)

Shown in Figure 6 is the comparison of the elliptic integral solution (Mattiasson, 1980) and that using elastofiber elements of the problem of the large deflection of an elastic cantilever beam with a vertical point load at its free end. The model is discretized into 10 elastofiber elements. The load  $P$  is increased, and the horizontal ( $u$ ) and vertical ( $w$ ) deflections of the free end are computed. These displacements are normalized by the length  $L$  and plotted against the load  $P$  normalized by  $EI/L^2$ . The close match demonstrates the geometric updating capabilities of the elastofiber element solution. The small error may be attributed to the omission of shear and axial deformations in the elliptic integral solution.

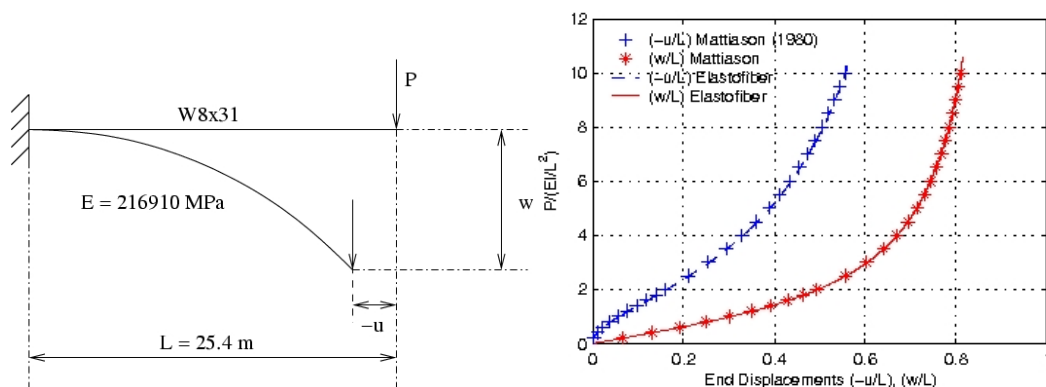


**Figure 6:** Comparison of free end horizontal and vertical displacements computed using 10 elastofiber beam elements against the analytical solution of an elastic cantilever beam subjected to a slowly increasing concentrated load at the free end.

### 2.2. Cyclic Lateral Loading of Cantilever Beam (Krishnan and Hall, 2006b)

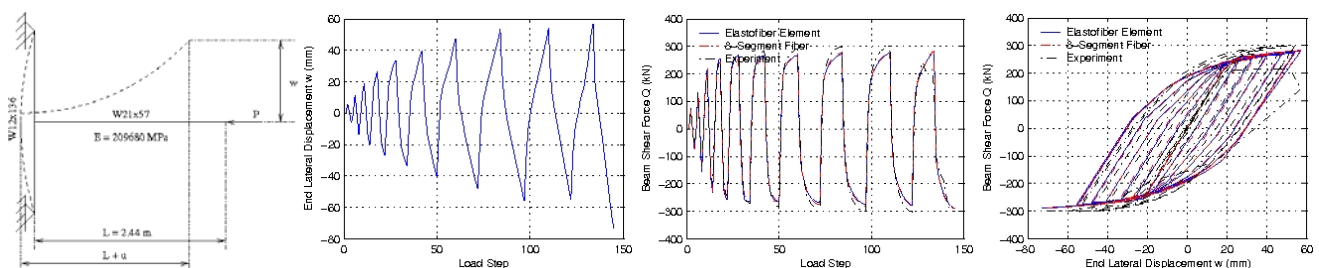


**Figure 7:** Cycled cantilever beam with applied lateral displacement history ( $P=0$ ). Comparison of numerical solutions using elastofiber (blue) and 2-D eight-segment fiber (red) elements against the experimental data.

Shown in Figure 7 is the comparison of the analytical solution using elastofiber and 2-D 8-segment fiber elements against the recorded response of a beam-column test setup subjected to a specified cyclic vertical displacement,  $w$ , at the free end (Engelhardt and Husain, 1993). The beam shear force ( $Q$ ) history and the

plot of  $Q$  versus  $w$  for the two beam elements match quite well, and agree with the experimental data up to the time that local flange buckling decreases the moment capacity of the test specimen (buckling occurs at load step 128). Even before this time, the response is well into the nonlinear range.

### 2.2. Cyclic Axial Loading of Steel Struts (Krishnan, 2008)

The measured axial load versus axial and lateral displacements of two steel struts, pinned at both ends, and subjected to quasi-static, axially applied, displacement and load reversal cycles (Black et al., 1980) are shown in the top row of Figure 8. Both struts were modeled using a single MEF element, as well as two elastofiber elements, and two plastic hinge elements for comparison. Ideal pinned-end and fixed-end conditions were assumed in the analysis. However, the initial geometric imperfection was adjusted in each case such that the initial buckling load matched the observed value. The initial buckling load is quite sensitive to support conditions and geometric imperfection, and in the absence of precise information about either quantity, fine-tuning of these two model parameters became imperative. With this initial tuning, the analytical models are able to very closely replicate the observed hysteretic behavior of all the struts, although they over-predict the residual compressive strength at the end of the cyclic tests. This is possibly because of cracking and fracture of the braces after a few loading cycles, that was unfortunately not recorded during the tests, and hence not included in the analysis either.

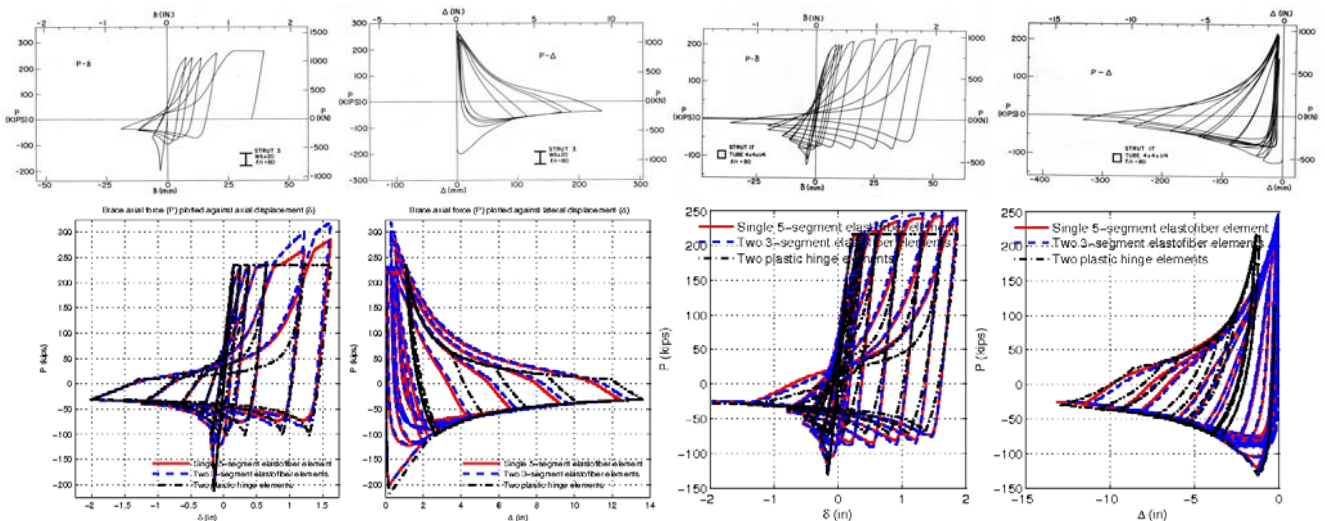


**Figure 8:** Axially loaded steel struts. Top row: Experimental axial force plotted against axial and lateral displacements for strut 3 (W6x20,  $L/r = 80$ ) and strut 17 (TS4x4x1/4,  $L/r = 80$ ), pinned at both ends. Bottom row: Analytical solution using one MEF element (red), two elastofiber elements (blue), and two plastic hinge elements (black).

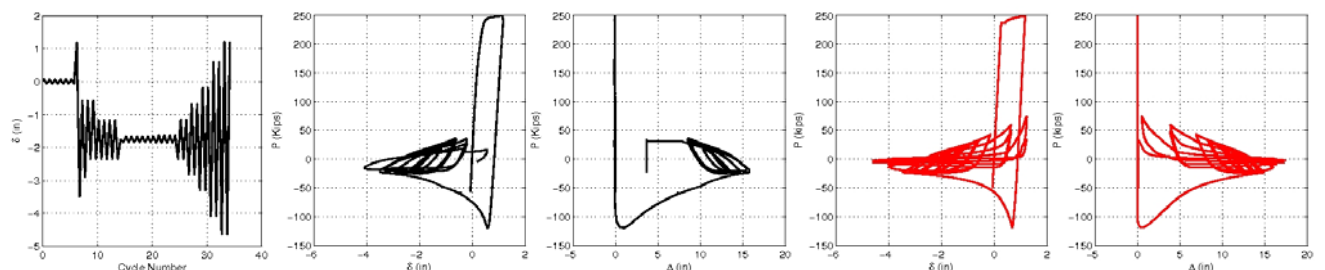


**Figure 9:** Near-fault asymmetric cyclic loading of a HSS 4x4x1/4 strut, tested under a NEESR project, and comparison of analytical solution (red) using a single modified elastofiber element against the measured response (axial displacement,  $\delta$ , and lateral displacement,  $\Delta$ , plotted against the axial force,  $P$ ) shown in black.

Fell et al. (2006) imposed a near-fault asymmetric cyclic axial displacement history to a steel strut and recorded its axial force and lateral displacement. Figure 9 shows a comparison of the analytical axial force-axial

displacement and axial force-lateral displacement histories using a single MEF element against the recorded data. The comparison looks quite good, although the nature of the hysteresis behavior observed in the experiment during tensile excursions is not captured accurately in the numerical model.

### 3. FRAMEWORK VALIDATION (Krishnan, 2008)

To validate FRAME3D's ability to simulate the response of an assembled structure, a full-scale six-story braced steel building that was designed, constructed, and tested at the Building Research Institute (BRI) in Tsukuba, Japan, under a US/Japan cooperative research program (Foutch et al. 1987, Roeder et al. 1987, Midorikawa et al. 1989) is modeled using FRAME3D. The test structure, designed in accordance with both US (UBC 1979) and Japanese design codes, consisted of three frames parallel to the direction of loading, and was subjected to the N-S component of the Tohoku University accelerogram recorded during the July 12, 1978, Miyagi-Ken-Oki earthquake, scaled to yield a peak acceleration of  $5.0 \text{ m/s}^2$ . Only one of the six bays of steel frames comprised steel braces, with the remaining comprising moment-frames. All beams, columns, and braces were modeled using MEF elements. Even though some model tuning was required to account for unexpected connection failures as well as fracture, the interstory drift ratio comparisons, and the interstory drift ratio--story shear hysteresis comparisons (Figure 10) are pretty good, and in general superior to former analytical studies (Midorikawa et al., 1989 and Tang & Goel, 1989).

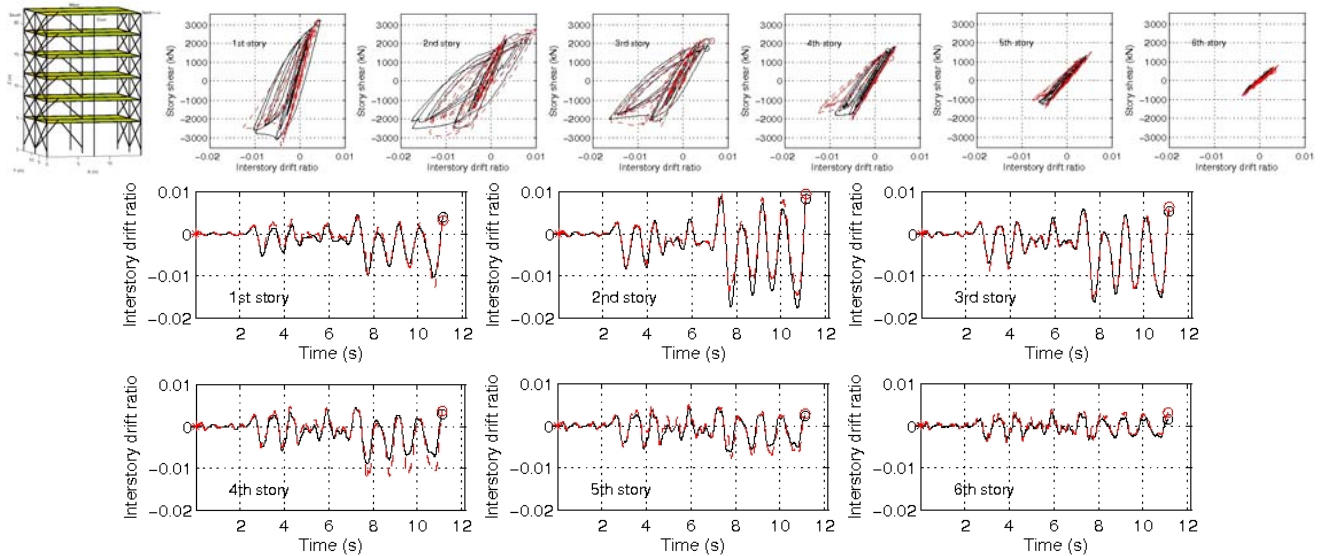


**Figure 10:** Comparison of the analytical and experimental response of the FRAME3D model of a six-story steel braced structure tested under the US-Japan cooperative research program.

## 4. EXAMPLES

### 4.1. Collapse of a Water Tank (Krishnan, 2008)

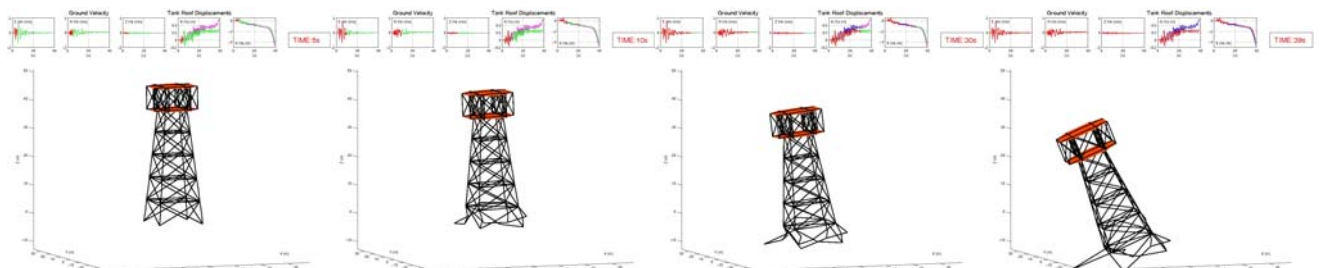


**Figure 11:** 5s, 10s, 30s, and 39s snapshots depicting the collapse of a steel water tank subjected to the Takatori near-source record from the 1995 Kobe earthquake.

A fictional water tank structure is subjected to the Takatori near-source record from the 1995 Kobe earthquake, scaled down by 0.75, to demonstrate FRAME3D's ability to simulate collapse. The snapshots of the deformed shape of the structure (Figure 11) indicate that the strong near-source pulse buckles the braces at the base and destabilizes the structure to such an extent that subsequent low-intensity shaking leads to total collapse of the tank.

#### 4.2. Analysis of Tall Steel Moment Frame Buildings Subjected to Simulated Ground Motion from an 1857-like Magnitude 7.9 San Andreas Fault Earthquake (Krishnan et al. 2006a, 2006b)

FRAME3D models of two 18-story steel moment frame buildings, one existing and the other fictional, are analyzed subjected to 3-component ground motion waveforms, computed at 636 analysis sites spread across southern California, from a simulated 1857-like magnitude 7.9 earthquake on the San Andreas fault. Shown in Figure 12 is a post-earthquake snapshot of the deformed shape of the two structures when located at the Northridge analysis site. The existing building model (orange), designed using the 1982 UBC is seen collapsing, whereas the fictional building model, designed using the 1997 UBC remains standing, although with a significant tilt to the west.

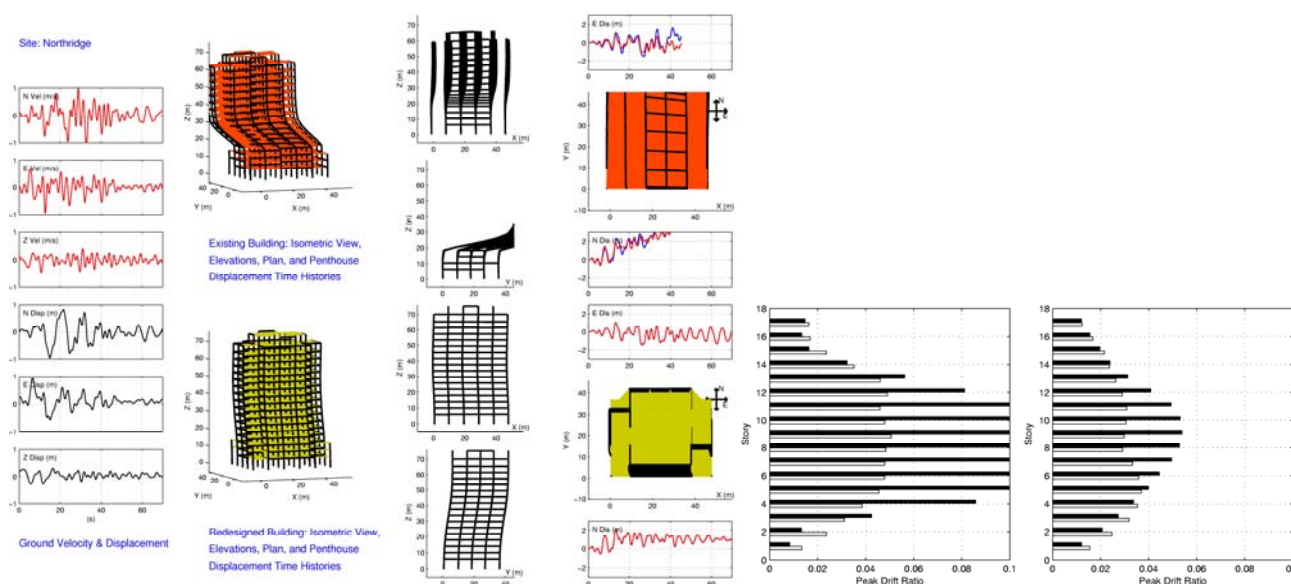


**Figure 12:** Snapshot of building deformation scaled up by a factor of 5 immediately following the earthquake at the Northridge analysis site for a hypothetical Mw 7.9 earthquake north-to-south rupture on the San Andreas Fault. Also shown are the time histories of the three components of the ground velocity and displacement bandpass-filtered between 2s and 1,000s using a Butterworth filter, the east and north components of the penthouse displacement of the existing and redesigned building models, and the peak drift in each of their stories.

#### REFERENCES

Black, G. R., Wenger, W. A. and Popov, E. P. (1980). Inelastic buckling of steel struts under cyclic load reversals. Tech. Rep. **UCB/EERC-80-40**, Earthquake Engineering Research Center, University of California, Berkeley.

Carlson, A. (1999). Three-dimensional nonlinear inelastic analysis of steel moment frame buildings damaged by earthquake excitations. Tech. Rep. **EERL 99-02**, Earthquake Engineering Research Laboratory, California Institute of Technology, Pasadena.

Challa, V. R. M. (1992). Nonlinear Seismic Behavior of Steel Planar Moment-Resisting Frames. Tech. Rep. **EERL 92-01**, Earthquake Engineering Research Laboratory, California Institute of Technology, Pasadena.

- Engelhardt, M. D. and Husain, A. S. (1993). Cyclic-loading performance of welded flange-bolted web connections. *Journal of Structural Engineering* **119:12**, 3537-3550.
- Fell, B. V., Kanvinde, A. M., Deierlein, G. G., Myers, A. T. and Fu, X. (2006). Buckling and fracture of concentric braces under inelastic cyclic loading. **Steel Tips: No. 94**, Structural Steel Educational Council.
- Foutch D. A., Goel, S. C. and Roeder, C. W. (1987). Seismic testing of full-scale steel building - Part I. *Journal of Structural Engineering* **113:11**, 2111-2129.
- Gan, W. and Hall, J. F. (1998). Static and dynamic behavior of steel braces under cyclic displacement. *Journal of Engineering Mechanics* **124:1**, 87-93.
- Hall (1995). Parameter study of the response of moment-resisting steel frame buildings to near-source ground motions. Tech. Rep. **EERL 95-08**, Earthquake Engineering Research Laboratory, California Institute of Technology, Pasadena.
- Hall (1998). Seismic response of steel frame buildings to near-source ground motions. *Earthquake Engineering and Structural Dynamics* **27:12**, 1445-1464.
- Hall and Challa (1995). Beam-Column Modeling. *Journal of Engineering Mechanics* **121:12**, 1284-1291.
- Krishnan, S. (2003). Three-Dimensional Nonlinear Analysis of Tall Irregular Steel Buildings Subject to Strong Ground Motion. Tech. Rep. **EERL 2003-01**, Earthquake Engineering Research Laboratory, California Institute of Technology, Pasadena.
- Krishnan, S. (2008). 3-D Modeling of steel braced structures. *Earthquake Engineering and Structural Dynamics* **Submitted**.
- Krishnan, S. and Hall, J. F. (2006a). Modeling steel frame buildings in three dimensions - Part I: Panel zone and plastic hinge beam elements. *Journal of Engineering Mechanics* **132:4**, 345-358.
- Krishnan, S. and Hall, J. F. (2006b). Modeling steel frame buildings in three dimensions - Part II: Elastofiber beam element and examples. *Journal of Engineering Mechanics* **132:4**, 359-374.
- Krishnan, S., Ji, C., Komatitsch, D. and Tromp, J. (2006a). Performance of two 18-story steel moment frame buildings in southern California during two large simulated San Andreas earthquakes. *Earthquake Spectra* **22:4**, 1035-1061.
- Krishnan, S., Ji, C., Komatitsch, D. and Tromp, J. (2006b). Case studies of damage to tall steel moment frame buildings in southern California during large San Andreas earthquakes. *Bulletin of the Seismological Society of America* **96:4**, 1523-1537.
- Mattiasson, K. (1980). Numerical results from large deflection beam and frame problems analyzed by means of elliptic integrals. *International Journal of Numerical Methods in Engineering* **17:1**, 145-153.
- Midorikawa, M., Nishiyama, I. and Yamanouchi, H. (1989). Analytical Evaluation of K-Braced Structure Seismic Test. *Journal of Structural Engineering* **115:8**, 1930-1948.
- Roeder, C. W., Foutch, D. A. and Goel, S. C. (1987). Seismic testing of full-scale steel building - Part II. *Journal of Structural Engineering* **113:11**, 2130-2145.
- Tang and Goel (1989). Brace fractures and analysis of phase I structure. *Journal of Structural Engineering* **115:8**, 1960-1976.